Hyperspectral *in vivo* two-photon microscopy of intrinsic contrast

Andrew J. Radosevich, Matthew B. Bouchard, Sean A. Burgess, Brenda R. Chen, and Elizabeth M. C. Hillman*

Laboratory for Functional Optical Imaging, Departments of Biomedical Engineering and Radiology, Columbia University, 1210 Amsterdam Avenue, New York, New York 10027, USA
**Corresponding author: eh2245@columbia.edu*

Received April 21, 2008; revised June 29, 2008; accepted July 16, 2008; posted August 13, 2008 (Doc. ID 95189); published September 12, 2008

In vivo two-photon imaging of intrinsic contrast can provide valuable information about structural tissue elements such as collagen and elastin and fluorescent metabolites such as nicotinamide adenine dinucleotide. Yet low signal and overlapping emission spectra can make it difficult to identify and delineate these species *in vivo*. We present a novel approach that combines excitation scanning with spectrally resolved emission two-photon microscopy, allowing distinct structures to be delineated based on their characteristic spectral fingerprints. The amounts of intrinsic fluorophores present in each voxel can also be evaluated. We demonstrate our method using *in vivo* imaging of nude mouse skin. © 2008 Optical Society of America

OCIS codes: 170.3880, 170.6900, 180.4315, 180.6900, 300.6410.

Two-photon microscopy allows high-resolution imaging of *in vivo* intact tissues. Intrinsic contrast from nicotinamide adenine dinucleotide (NADH), flavin adenine dinucleotide (FAD), collagen, elastin, and keratin [1–3] can allow measurement of metabolism and native structure without the need to introduce artificial compounds. However, analysis of intrinsic fluorophores (and some exogenous contrast agents) is complicated by their broad overlapping emission spectra [4,5]. Reliable imaging of intrinsic contrast on microscopic-length scales in tissues such as the heart, brain, skin, and tumors could provide important insights into cellular function and allow improved interpretation and validation of diagnostics based on *in vivo* bulk-tissue measurements [3]. In this Letter we demonstrate a hyperspectral two-photon data acquisition and spectral unmixing technique that can delineate and quantify the concentrations of multiple intrinsic fluorophores and sources of second-harmonic generation (SHG) *in vivo*. We show that limited spectral data can be used to segment distinct structures within 3D volumes, based on the specific excitation–emission fingerprints of each structure's constituents. We also demonstrate that hyperspectral microscopy can allow extraction of the relative concentrations of specific intrinsic fluorophores, effectively yielding *in vivo*, spatially resolved chemical analysis of fine submicrometer structure.

All measurements were made using our home-built two-photon microscope system, which includes three photomultiplier detectors (350–505 nm, 505–560 nm, and 560–650 nm emission ranges, R3896 Hamamatsu), a Ti:sapphire laser (MaiTai XF, Spectra Physics), and an Olympus XLUMPlanFl $20\times/0.95$ W objective, mounted on a fine z-adjustment stage (M-112.1DG, PI). Our integrated control software written in MATLAB allows synchronous tuning of the laser wavelength during imaging [6].

Three male nude mice (40–45 g) were anesthetized with isoflurane and positioned on a warming pad on the microscope's x–y stage. One ear was moistened with water and held flat between a microscope slide and a glass cover slip. Data sets were acquired in two ways: Wavelength scans consisted of 400×400 pixel images captured in synchrony with the laser being tuned from 710 to 920 nm in 2 nm steps and depth-resolved image stacks were acquired every 3 μm to a depth of 100 μm at excitation wavelengths of 720 nm, 800 nm, and then 900 nm. Acquisition of these scan sets took 180 and 120 s, respectively.

The detected two-photon fluorescence of a mixture of fluorophores can be assumed to be a linear sum of the fluorescence of each species [7]:

$$F_{\mathrm{mix}} = K\sum_n \phi_n \eta_n \sigma_n C_n, \tag{1}$$

where C is the fluorophore concentration, $\eta(\lambda_{ex},\lambda_{em})$ is the fluorophore quantum efficiency, $\phi(\lambda_{em})$ is the fluorescence collection efficiency, $\sigma(\lambda_{ex})$ is the two-photon absorption cross section, and $K(\lambda_{ex}) = P^2\pi^2 \mathrm{NA}^4/(2\tau_p f_p^2 h^2 c^2 \lambda_{ex}^2)$, where $P(\lambda_{ex})$ is the laser power, $\tau_p(\lambda_{ex})$ is the excitation pulse width, f_p is the laser duty cycle, $\mathrm{NA}(\lambda_{ex})$ is the lens NA, λ_{ex} is the excitation wavelength, c is the speed of light, h is Planck's constant. SHG will add to this signal, and can be approximated as $(P^2/\tau_p)\Sigma_n B_n(\lambda_{ex},\lambda_{em})S_n^2$, where S_n is the density of SHG-active molecules and B_n is a function of the material type [8]. Assuming that K is spatially and temporally invariant, linear unmixing strategies can therefore be applied to multispectral two-photon data. Images of C_n and S_n^2 can be calculated via a nonnegative least-squares fit to both "seeded" basis spectra, and basis spectra of intrinsic fluorophores measured *in vitro*.

Figures 1(a)–1(c) show an example of spectrally unmixed data using "seed regions." In our depth-resolved stack data, each voxel effectively contains a coarse nine-element excitation–emission map consisting of 720, 800, and 900 nm excitations and 350–505, 505–560, and 560–650 nm emissions. Six seed regions were selected from this data set, targeting regions with distinctive morphology. The spectra extracted from these regions were then fit to the spectrum of every voxel, thereby identifying all areas

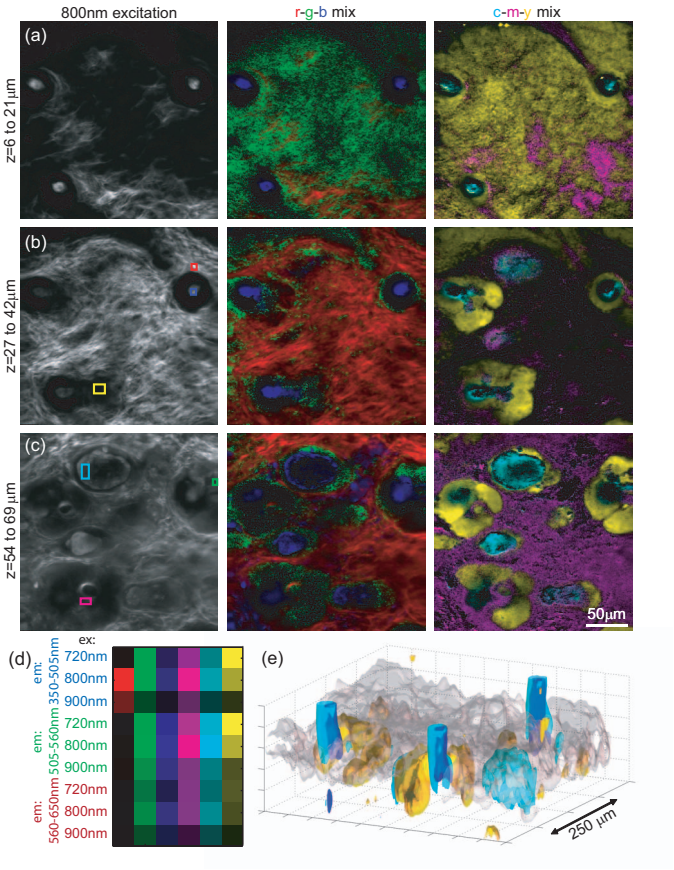

Fig. 1. *In vivo* 3D hyperspectral unmixing using seed regions. Rows (a), (b), and (c) show different depth slices in the skin. Left, 350–505 nm emission images for 800 nm excitation with seed regions indicated; center and right, color merges of the six unmixed component images. (d) Nine-element basis spectra of the seed regions (shown on linear colormaps). (e) 3D isosurface rendering of unmixed data (yellow, blue, cyan, and red=gray components shown). Multimedia supplements: RGB–CMY stack movie (Media 1); raw data, fit, and fit residuals movie (Media 2); conventional histology (Media 3).

composed of material similar to that in each seed region. Unmixing results are shown at three different depths, with three unmixed components merged as red–green–blue (RGB), and three as a cyan–magenta–yellow (CMY) merges. These images reveal keratinocytes in the epidermis and the hair follicle sheath (yellow), fibrous structures in the dermis (red), hairs (blue), sebaceous glands (yellow), and hair follicle cysts (common in hairless mice—cyan). Figure 1(e) shows a 3D isosurface rendering of four of these fit components. The spectral basis sets are represented in Fig. 1(d). Additional species can be delineated if more regions are seeded, including blood vessels and the separation of epidermal keratinocytes from sebaceous glands.

This seeding approach allows image contrast to be enhanced without exogenous labeling and could also allow automated isolation, counting, and volumetric measurement of physiologically distinct regions without complex 3D segmentation algorithms or histological slice coregistration. This example used only a 3×3 excitation–emission subset. Unmixing can also be achieved using more excitation wavelengths and a single emission channel [6]. In general, delineation is successful when each seeded tissue type has a unique excitation–emission spectrum. However, because seeded spectra are likely to contain a mixture of several compounds, it is important to seed enough regions to allow the whole data set to be represented by the fit, with low residuals.

An alternative approach is to fit instead to the basis spectra of all of the fluorophores (and SHG species) expected within the tissue. This has the significant benefit of allowing voxel-by-voxel quantification of the chemical composition of structures within living tissue. We obtained *in vitro* purified samples of the major intrinsic fluorophores expected in skin: NADH, FAD, tryptophan, elastin, keratin, and collagen I (N8129, F6625, T9753, E1625, and K0253 from Sigma-Aldrich and CB-40236 from Fisher Sciences) [3]. Most samples were prepared at 5 mM in phosphate-buffered saline (PBS). Collagen was gelled in PBS and 1N NaOH, and elastin was hydrated in PBS. Each sample was imaged on a glass slide using 2 nm spaced excitation wavelength scans. The SHG spectra of fibrils of collagen and crystalline keratin were isolated from their fluorescence spectra in solution. Tryptophan fluorescence was not detected. The extracted excitation–emission basis spectra were then fit to *in vivo* wavelength scan data. In our first fit, the sebaceous gland fit strongly to NADH, but upon inspection, the seeded spectrum differed from NADH, and sebum is known to be fluorescent [9]. In lieu of a pure sample, we repeated the fit, including a seeded sebaceous gland spectrum. The resulting images represent maps of the concentration of each intrinsic fluorophore in each voxel (Fig. 2). The bar graph shows the maximum scale of each map and the compositions of three regions: a sebaceous gland, a hair root, and the surrounding dermis.

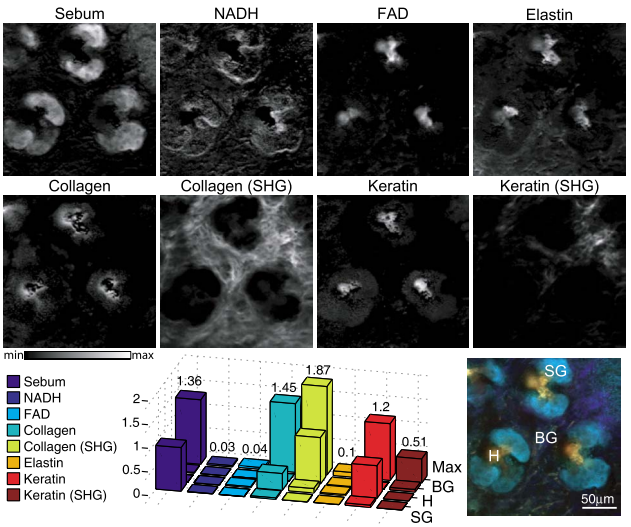

Fig. 2. (Color online) *In vivo* maps of intrinsic fluorophore concentration. Each voxel was calculated using nonnegative least-squares fitting to basis spectra of pure samples of intrinsic fluorophores. Below, Max, maximum fit contrast for each map; SG, sebaceous gland; H, hair; BG, background. Amplitudes are fractions with respect to the concentrations of the *in vitro* solutions. Multimedia supplement: raw wavelength scan movie (Media 4).

We repeated this analysis at other skin areas and depths, finding good agreement in the morphology of each map with respect to the structures in the skin. However, it should be noted that these images, as the first of their kind (to our knowledge), are difficult to validate. Residuals of this fit were larger than for the seeded basis spectra, and we suspect cross talk between keratin and FAD, as well as overlap between sebum and NADH (since the seeded sebum spectrum likely contains NADH). Since only type I collagen was included, the "keratin SHG" image may instead represent SHG of other collagen species. *In vitro* spectra may also differ from the spectra of these compounds *in vivo*, where environments and binding may be different (a problem faced by almost all *in vivo* spectroscopy analysis). Refining our basis spectra and seeking further ways to test and validate these results are priorities in our ongoing work.

To validate the primary assumptions of this approach [as given by Eq. (1)], we performed *in vitro* measurements of mixtures of pure samples of NADH and FAD in PBS (NADH:FAD ratios 500:0 μM, 375:25 μM, 250:50 μM 125:75 μm and 0:100 μm). Figures 3(a) and 3(b) compare the one-photon (using Jobin Yvon Skinskan) and two-photon spectra of pure NADH and FAD. Figure 3(c) shows the result of nonnegative least-squares fitting of these basis spectra to the spectrum of each mixture. These fits used only the 505–560 and 560–650 nm emission channels, since in a concentrated solution FAD strongly absorbs the blue light emitted by NADH. The same effect still causes the slight exponential weighting of the NADH concentrations, although this can be corrected by including second- and third-order terms in our fits (not shown). *In vivo*, NADH is more prevalent than FAD; however, care should be taken to ensure that absorption of emitted light (particularly if dyes are present) is considered when fitting to excitation–emission data. Excitation-spectrum unmixing is inherently more tolerant of these effects than emission-spectrum fitting and unmixing. Overall, we find good agreement between the true and retrieved concentrations of each intrinsic fluorophore, supporting our *in vivo* quantitative analysis results.

The raw two-photon excitation spectra shown in Fig. 3 are modulated by a repeatable wavelength-dependent pattern. These variations in two-photon excitation efficiency reflect the wavelength-dependence of system parameters denoted by $K(\lambda_{ex})$. We expect that our system's response is primarily due to dispersion within our optical elements. In their demonstration of unmixing of two-photon excitation spectra in stained, *ex vivo* samples, Dickinson *et al.* [7] evaluated the pulse-width variation of their laser but calibrated only for power variations. Albota *et al.* [10] measured the two-photon excitation spectra of biomolecular probes at 20 nm intervals and calibrated using fluorescein as a standardization reference. We found that if excitation light leakage is minimized, $K(\lambda_{ex})$ remains constant between *in vitro* and *in vivo* measurements, such that correction for this multiplicative factor is not necessary. While this means that all samples must be measured on the same system, self-cancellation of this factor appears to be more accurate than calibration using reference standards or single-photon spectra.

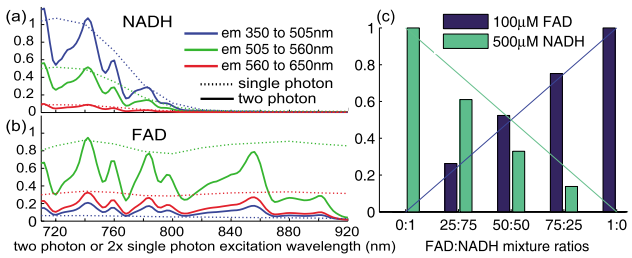

Fig. 3. (Color online) *In vitro* validation. (a), (b) Single- and (uncorrected) two-photon excitation spectra of NADH and FAD for three emission bands. (c) Results of nonnegative least-squares fits for *in vitro* mixtures.

In summary, by acquiring hyperspectral two-photon data from which spectral signatures of each voxel can be extracted, physiologically meaningful structures can be delineated within a living sample with submicrometer resolution. The relative amounts of constituent fluorophores within living cells can also be quantified. This method capitalizes on the tunability of most modern Ti:sapphire lasers and offers enhanced contrast in the absence of exogenous agents and the possibility of quantitatively mapping cellular metabolism *in vivo*.

We acknowledge support from National Institutes of Health (NIH) grants R21NS053684 and R01NS063226, the Human Frontier Science Program, the Wallace H. Coulter Foundation, and the Rodriguez family. We thank Rebecca Morris, Angela Christiano, and David Owens.

References

1. W. R. Zipfel, R. M. Williams, R. Christie, A. Y. Nikitin, B. T. Hyman, and W. W. Webb, Proc. Natl. Acad. Sci. USA **100**, 7075 (2003).
2. S. Huang, A. A. Heikal, and W. W. Webb, Biophys. J. **82**, 2811 (2002).
3. N. Ramanujam, in *Encyclopedia of Analytical Chemistry*, R. A. Meyers, ed. (Wiley, 2000), Vol. 1, pp. 20–56.
4. J. A. Palero, H. S. de Bruijn, A. van der Ploeg-van den Heuvel, H. J. C. M. Sterenborg, and H. C. Gerritsen, Opt. Express **14**, 4395 (2006).
5. J. R. Mansfield, K. W. Gossage, C. C. Hoyt, and R. M. Levenson, J. Biomed. Opt. **10**, 041207 (2005).
6. A. J. Radosevich, M. B. Bouchard, S. A. Burgess, R. Stolpher, B. Chen, and E. M. C. Hillman, in *Biomedical Optics*, OSA Technical Digest (CD) (Optical Society of America, 2008), paper BW67.
7. M. E. Dickinson, E. Simbuerger, B. Zimmermann, C. W. Waters, and S. E. Fraser, J. Biomed. Opt. **8**, 329 (2003).
8. P. J. Campagnola, H. A. Clark, W. A. Mohler, A. Lewis, and L. M. Loew, J. Biomed. Opt. **6**, 277 (2001).
9. B. Han, B. Jung, J. S. Nelson, and E.-H. Choi, J. Biomed. Opt. **12**, 014006 (2007).
10. M. A. Albota, C. Xu, and W. W. Webb, Appl. Opt. **37**, 7352 (1998).